JACS
JOURNAL OF THE AMERICAN CHEMICAL SOCIETY
pubs.acs.org/JACS
Article

Quantum Defects: What Pairs with the Aryl Group When Bonding to the sp^2 Carbon Lattice of Single-Wall Carbon Nanotubes?

Peng Wang, Jacob Fortner,[‖] Hongbin Luo,[‖] Jacek Kłos, Xiaojian Wu, Haoran Qu, Fu Chen, Yue Li, and YuHuang Wang*

Cite This: *J. Am. Chem. Soc.* 2022, 144, 13234−13241
Read Online
ACCESS | Metrics & More | Article Recommendations | Supporting Information

ABSTRACT: Aryl diazonium reactions are widely used to covalently modify graphitic electrodes and low-dimensional carbon materials, including the recent creation of organic color centers (OCCs) on single-wall carbon nanotube semiconductors. However, due to the experimental difficulties in resolving small functional groups over extensive carbon lattices, a basic question until now remains unanswered: what group, if any, is pairing with the aryl sp^3 defect when breaking a C═C bond on the sp^2 carbon lattice? Here, we show that water plays an unexpected role in completing the diazonium reaction with carbon nanotubes involving chlorosulfonic acid, acting as a nucleophilic agent that contributes −OH as the pairing group. By simply replacing water with other nucleophilic solvents, we find it is possible to create OCCs that feature an entirely new series of pairing groups, including $-OCH_3$, $-OC_2H_5$, $-OC_3H_7$, *-i*-OC_3H_7, and $-NH_2$, which allows us to systematically tailor the defect pairs and the optical properties of the resulting color centers. Enabled by these pairing groups, we further achieved the synthesis of OCCs with sterically bulky pairs that exhibit high purity defect photoluminescence effectively covering both the second near-infrared window and the telecom wavelengths. Our studies further suggest that these diazonium reactions proceed through the formation of carbocations in chlorosulfonic acid, rather than a radical mechanism that typically occurs in aqueous solutions. These findings uncover the unknown half of the sp^3 defect pairs and provide a synthetic approach to control these defect color centers for quantum information, imaging, and sensing.

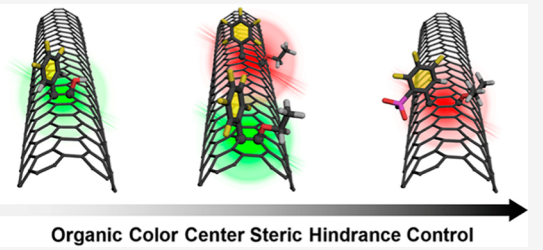

INTRODUCTION

Aryl diazonium chemistry is a versatile family of synthetic reactions[1−3] that have been widely used for surface functionalization of graphitic electrodes,[4,5] band gap engineering of graphene,[6] synthesis of new composite materials,[7] and most recently, the creation of organic color centers (OCCs) in semiconducting single-wall carbon nanotubes (SWCNTs).[8] All of these applications are based on the fact that the diazonium reaction covalently attaches aryl functional groups to the graphitic carbon surface, creating sp^3 defects in the sp^2-hybridized lattice. At low functional density, these sp^3 defects emerge as OCCs that fluoresce brightly in the shortwave infrared,[8] with emissions that are single-photon in nature, even at room temperature.[9] Notably, this defect photoluminescence (PL) is energetically distinct for each individual OCC structure,[8] in which the sp^3 defects act as exciton traps that produce fascinating photophysics and chemical properties.[10,11] As a result, OCCs are being intensively studied and exploited for applications in imaging,[12] sensing,[13] and quantum technologies.[9,14,15] However, the mechanism of the diazonium reaction is complex on the extensive sp^2 carbon lattice, with questions of fundamental importance that remain unanswered.

The diazonium reaction with graphitic carbons in aqueous solutions are known to begin with the transfer of an electron from the nanocarbon to the aryl diazonium reactant,[2,16] which displaces the diazonium group (leaving as N_2) leading to the formation of a C−C σ bond and therefore an sp^3 defect in the sp^2-hybridized carbon lattice. The bonding of the aryl functional group presumably leaves a radical on an adjacent carbon atom, which is assumed to further react with other species available in solution to maintain the neutral closed-shell configuration, thus forming a second pairing group.[2,17] A hydrogen atom is often used as the pairing group in theoretical modeling studies, including those on OCCs.[18−20] However, the existence and the chemical nature of this pairing group remains experimentally unconfirmed due to experimental difficulties, with several possibilities proposed, including −H, −OH, or another aryl moiety (Figure 1a).[8,19,21] Furthermore, due to the conjugation nature of the sp^2 carbon lattice, it is hypothesized that the unbalanced radical can delocalize *via* resonance until it eventually reacts with a pairing group to

Received: April 10, 2022
Published: July 13, 2022

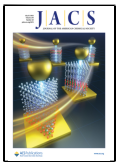

https://doi.org/10.1021/jacs.2c03846
J. Am. Chem. Soc. 2022, 144, 13234−13241

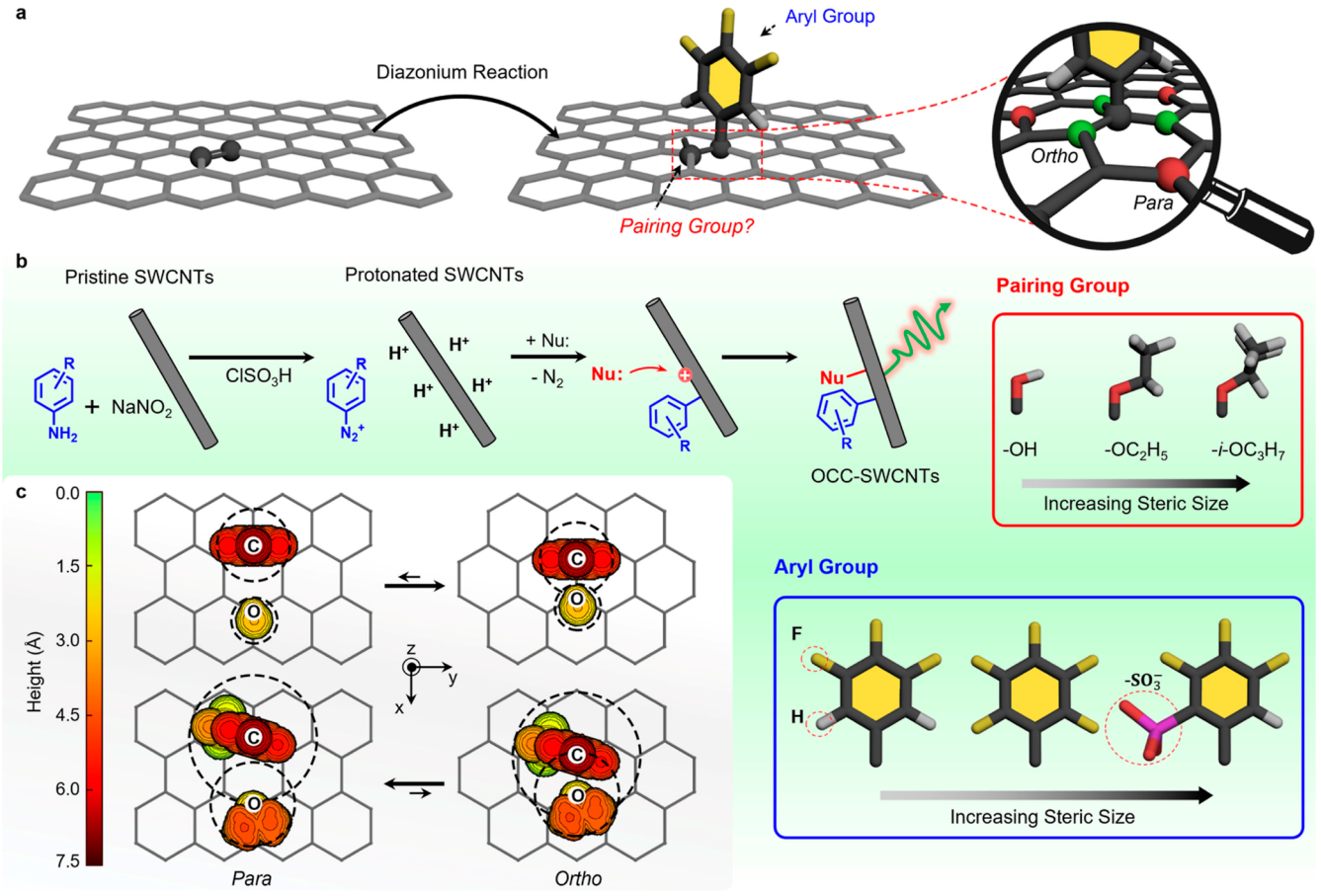

Figure 1. Solvents control the pairing group in the aryl diazonium reaction with sp^2 carbon. (a) Reaction scheme for the covalent functionalization of sp^2 carbon by aryl diazonium chemistry. 3,4,5-Trifluorobezene diazonium is shown as an example. The chemical identity of the pairing group is not known, nor its bonding position relative to the aryl group. (b) Proposed synthetic route to incorporate different types of aryl and pairing groups. Nu: represents different types of nucleophilic solvents (e.g., H_2O and C_2H_5OH) that are used in the reaction. (c) Steric topology maps (top view) of the defect pairs (using 3F-Ar/OH and 3F−SO_3-Ar/OCH$(CH_3)_2$ as examples) superimposed on a sp^2 lattice. The steric hindrance of the 3F-Ar/OH defect pair can be accommodated by the ortho configuration, whereas the larger 3F-SO_3-Ar/OCH$(CH_3)_2$ pair can only adopt a para configuration. Note: the steric topology map of 5F-Ar, whose size is in between 3F-Ar and 3F-SO_3-Ar, is not shown for clarity.

form a stable OCC.[19,22] Based on the charge localization predicated by density functional theory (DFT) calculations, the aryl and pairing groups may likely adopt one of the six closely paired atomic bonding configurations on the SWCNT (three ortho and three para, Figure 1a),[23] each having different exciton trapping potential and corresponding defect PL.[19,22] Such structural variability enriches the family of OCCs, but it also results in complex and inhomogeneous distribution of the OCC emissions, which poses a significant synthetic challenge to applications such as single-photon quantum light sources where identical emitters are required for scaling.[24] Despite recent advances in addressing this structural control issues by others and us,[25,26] such structural variability remains an outstanding question at this frontier which provide another motivation for identifying the pairing groups.

Herein, we show that water plays an unexpected role in completing the diazonium chemistry with SWCNTs in chlorosulfonic acid by acting as a nucleophilic agent and providing −OH as the pairing group. Applying this new insight, we designed experiments to control both the aryl and pairing groups of an OCC with diazonium chemistry by breaking it into two processing steps (Figure 1b). We first co-dissolve SWCNTs in chlorosulfonic acid along with an aniline and sodium nitrite ($NaNO_2$), to in situ synthesize a diazonium salt, or alternatively we can directly add a pre-synthesized diazonium salt.[27] We then introduce this acidic solution to a nucleophilic solvent, which we find is crucial to complete the reaction and control the pairing group, affording OCCs that feature an entirely new series of pairing groups, including hydroxy (−OH), methoxy (−OCH_3), ethoxy (−OC_2H_5), *n*-propoxy (−OC_3H_7), *i*-propoxy (−*i*-OC_3H_7), and amino (−NH_2) groups. The PL of the synthesized OCCs provides a spectral fingerprint that allows us to experimentally track and follow the reactions, which otherwise would be experimentally difficult to probe in these low concentration and heterogeneous conditions. We find that the defect PL systematically narrows and red-shifts with sterically larger aryl and pairing groups. This trend holds for all tested semiconducting SWCNT hosts of different chiralities and diameters. Steric hindrance and DFT calculations reveal that as the steric hindrance increases, the atomic configurations adopted by the defect pair shifts from the ortho to para positions on the sp^2 carbon lattice (Figure 1c). Controlling this steric hindrance effect through judicious choice of bulky functional group pairs leads to a significantly red-shifted, single OCC PL peak that effectively covers the spectral windows for both NIR II bioimaging and telecom communications. This study thus provides key insights in understanding the diazonium

https://doi.org/10.1021/jacs.2c03846
J. Am. Chem. Soc. 2022, 144, 13234−13241

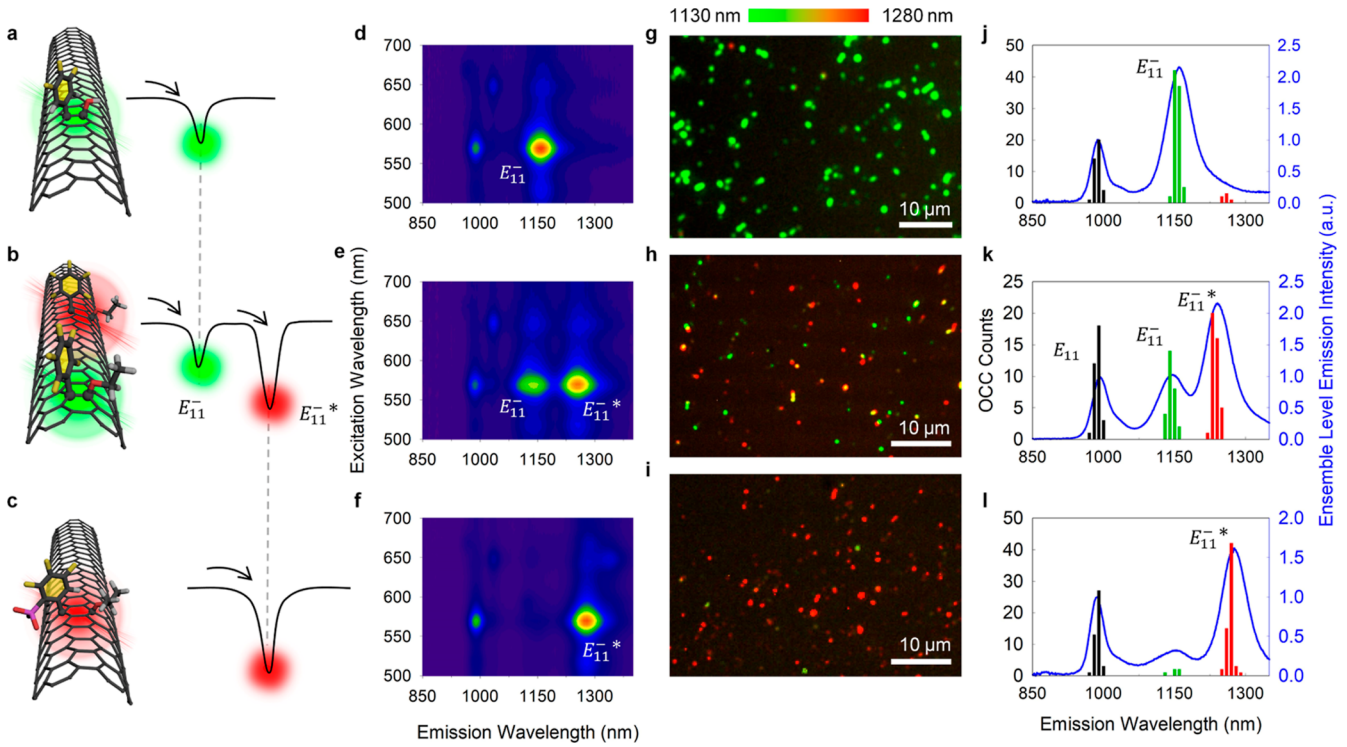

Figure 2. Both the aryl and pairing groups have a strong impact on the optical properties of OCCs. (a–c) OCCs on a semiconducting SWCNT create sterically controlled exciton traps that efficiently harvest and convert nanotube excitons into E_{11}^- and E_{11}^-* PL (labeled in green and red, respectively). (d–f) Representative excitation–emission PL maps of OCC-(6,5)-SWCNTs with (d) 3F-Ar/OH, (e) 5F-Ar/OCH_2CH_3, and (f) 3F–SO_3-Ar/*i*-OC_3H_7 defect pairs. (g–i) Hyperspectral PL images and (j–l) PL peak distribution histograms of OCC-(6,5)-SWCNTs with (g,j) 3F-Ar/OH, (h,k) 5F-Ar/OCH_2CH_3, and (i,l) 3F–SO_3-Ar/*i*-OC_3H_7 defect pairs. The PL images are false-colored to indicate the emission wavelength range: green (1130–1180 nm) and red (1210–1280 nm). Scale bars are 10 μm. The blue curves in j–l are the ensemble-level room temperature PL spectra of the corresponding OCC-(6,5)-SWCNTs dispersed in 2% DOC D_2O solution.

chemistry of graphitic materials and significantly expands our toolsets for controlling defect color centers.

RESULTS AND DISCUSSION

To generate the OCCs, we first dissolve the SWCNTs in chlorosulfonic acid, followed by the addition of $NaNO_2$ and an aniline, such as 3,4,5-trifluoroaniline. We confirmed by ^{19}F NMR spectroscopy that the aniline and $NaNO_2$ react in the superacid to form 3,4,5-trifluoroaryl (3F-Ar) diazonium species (see Figure S1 and Supporting Information for more details). We then added the acidic mixture containing the SWCNTs and diazonium drop-by-drop to Nanopure water, in which the SWCNTs precipitate as black aggregates (Figure S2a) that can be readily redispersed and stabilized as individual SWCNTs in water by sodium deoxycholate (DOC) surfactant. The resulting aqueous solution (Figure S2b) displays defect-induced PL (E_{11}^- at ~1160 nm, Figure S2c), signaling the successful incorporation of the OCCs on the SWCNT sidewalls (hereafter referred as OCC-SWCNTs).[8]

Control experiments in the absence of aniline or $NaNO_2$ failed to produce OCCs, as indicated by the lack of defect PL emission, in addition to no increase in the disordered (*D*) peak at ~1300 cm^{-1} in the Raman spectrum (Figure S3). Unexpectedly, however, we found that without H_2O, the reaction did not occur either, even if heated to 100 °C (Figure S3). The need for H_2O to drive this reaction was unexpected as Hudson et al. have previously reported that such diazonium reactions occur directly in the superacid media and that heating and radical initiators are needed to trigger the reaction.[28] To further investigate the possibility that this acidic diazonium chemistry does not proceed through a radical-mediated pathway, as previously believed, we added an excess amount of (2,2,6,6-tetramethylpiperidin-1-yl)oxidanyl (TEMPO), a radical inhibitor,[29] to the water that was introduced into the mixture. We note that TEMPO was added to water instead of chlorosulfonic acid because it would decompose in the superacid. Under these conditions, we found the reaction still occurred (Figure S4), which is against the radical mechanism. These findings indicate that the acidic diazonium chemistry is neither radical-initiated, nor does it solely occur in the superacid medium, as adding the chlorosulfonic acid solution to water is required to achieve the covalent functionalization reaction that produces the OCCs.

Based on these results, we propose this acidic diazonium reaction may proceed instead through electrophilic addition. When bonding to the nanotube in the presence of chlorosulfonic acid, the aryl group leaves an adjacent carbocation on the sp^2 carbon lattice that subsequently reacts with water, which acts as a nucleophile to form a covalent bond that completes the OCC defect pair (Figure 1b and Scheme S1). Indeed, at low pH, carbocations, rather than carbon radicals, form more favorably from diazonium species.[30] However, the covalent reaction between the diazonium species and the SWCNTs does not occur until water is available. Instead, the cationic diazonium reactant appears to physically adsorb on the SWCNT surface in the superacid, rather than bonding covalently, as evidenced by a strong resonance

https://doi.org/10.1021/jacs.2c03846
J. Am. Chem. Soc. 2022, 144, 13234–13241

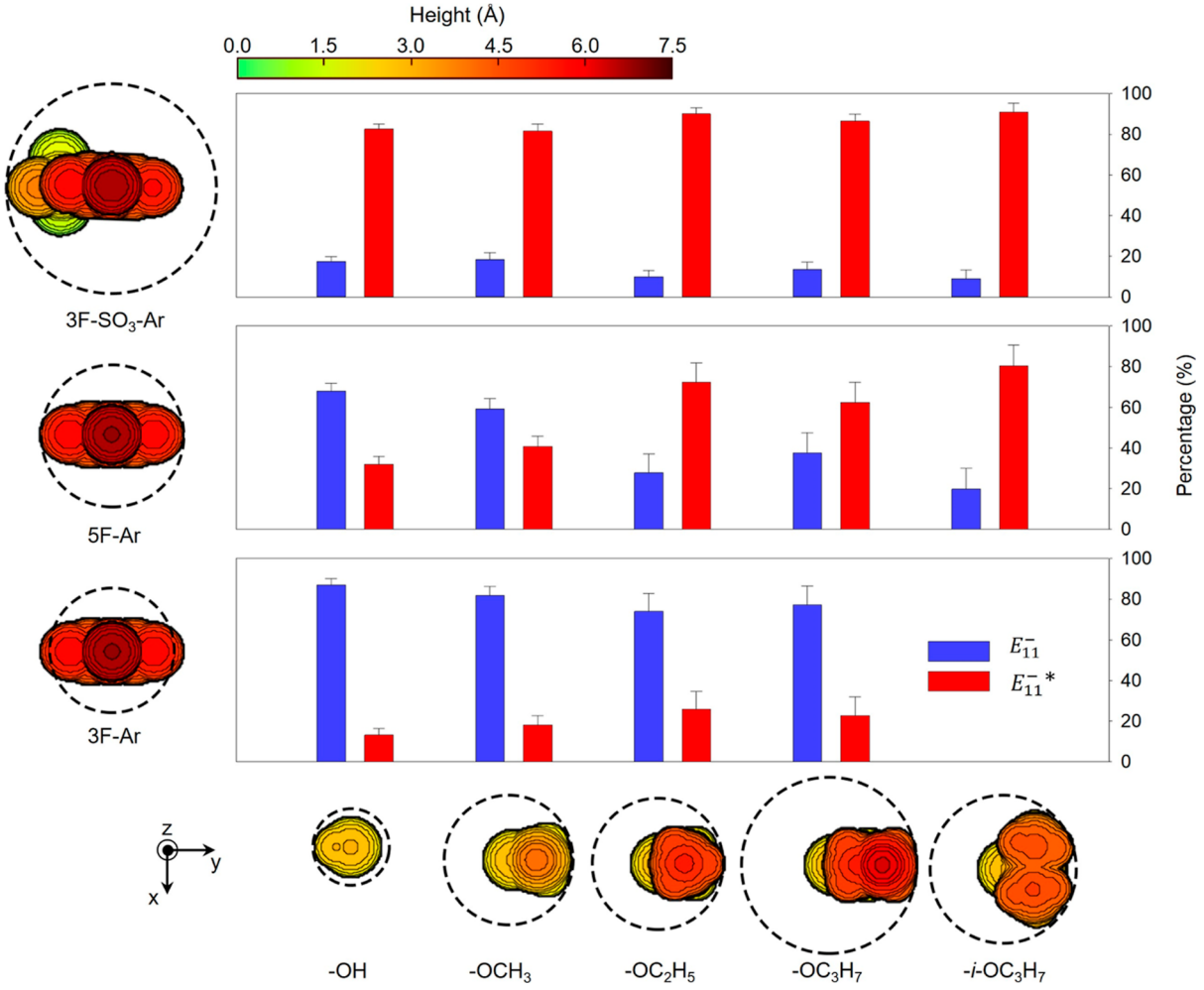

Figure 3. Steric control of defect PL. The ratio of the integrated E_{11}^{-} (blue) and E_{11}^{-}* (red) emissions of OCC-(6,5)-SWCNTs strongly depends on the relative steric sizes of the aryl group (including 3F-Ar, 5F-Ar, and 3F-SO_3-Ar) and the pairing group (including −OH, $-OCH_3$, $-OC_2H_5$, $-OC_3H_7$, and $-i$-OC_3H_7). The functional groups are presented as steric topology maps to show their relative steric sizes. The radii of the functional groups are indicated by the dashed circles.

broadening effect observed in the ^{1}H NMR spectrum (Figure S5).

We further show that this unexpected role of water as a nucleophile in this reaction can be generalized to other solvents of different steric sizes and electronic characteristics, allowing us to control the OCC pairing group. We found that a wide variety of nucleophilic solvents, including methanol, ethanol, *n*-propanol, and liquid ammonia, readily participate in this OCC generation chemistry (Figure S6a−e). The OCCs synthesized from these solvents generate defect PL (E_{11}^{-}) whose peak wavelength is influenced by the chemical nature of the pairing group, particularly by the type of the atom that is directly bonded to the carbon lattice. Specifically, pairing groups that bond to the SWCNTs *via* oxygen atoms (including −OH, $-OCH_3$, $-OC_2H_5$, $-OC_3H_7$) result in similar E_{11}^{-} emission at ∼1158 nm for 3,4,5-trifluorobenzene OCC-tailored (6,5)-SWCNTs, with a small variance of only ∼5 nm. In contrast, pure liquid ammonia showed a less red-shifted peak at ∼1138 nm, which is consistent with a more electron-donating $-NH_2$ pairing group bonded to the SWCNT through a C−N bond (Figure S6f).

These results suggest that the pairing group provides an electronic contribution to the trapping depth of the resulting OCC, which is supported by our DFT calculations. We modeled (6,5)-SWCNTs with an individual OCC composed of a 3F-Ar and a pairing group of either −OH, $-OCH_3$, $-OC_2H_5$, or $-NH_2$, then performed ground-state geometry optimization and time-dependent DFT to find the optical transitions associated with the attached OCC (see the Supporting Information for details). We found similar optical transitions (variance <5 meV) for all three O-bonded pairing groups (−OH, $-OCH_3$, and $-OC_2H_5$). However, the optical transition for 3F-Ar paired with the $-NH_2$ group (designated as 3F-Ar/NH_2) was ∼20 meV less red-shifted (Figure S7). We note the $-NH_2$ case takes place at −40 °C in liquid ammonia, and the impact of this low temperature is not known. These relative energies predicted by DFT match the differences found in the experimental PL peaks for reactions where water, methanol, ethanol, or liquid ammonia was used as the nucleophilic solvent (Figure S8), which supports our conclusion that the pairing group for the OCC is determined by the choice of nucleophilic solvent.

We also tested solvents that are weak or non-nucleophilic, including acetone, tetrahydrofuran, and others, as shown in Figure S9. However, these solvents were unable to trigger the reaction. Sterically bulky nucleophilic solvents, such as *tert*-butanol, were also ineffective, which may be attributed to their

https://doi.org/10.1021/jacs.2c03846
J. Am. Chem. Soc. 2022, 144, 13234−13241

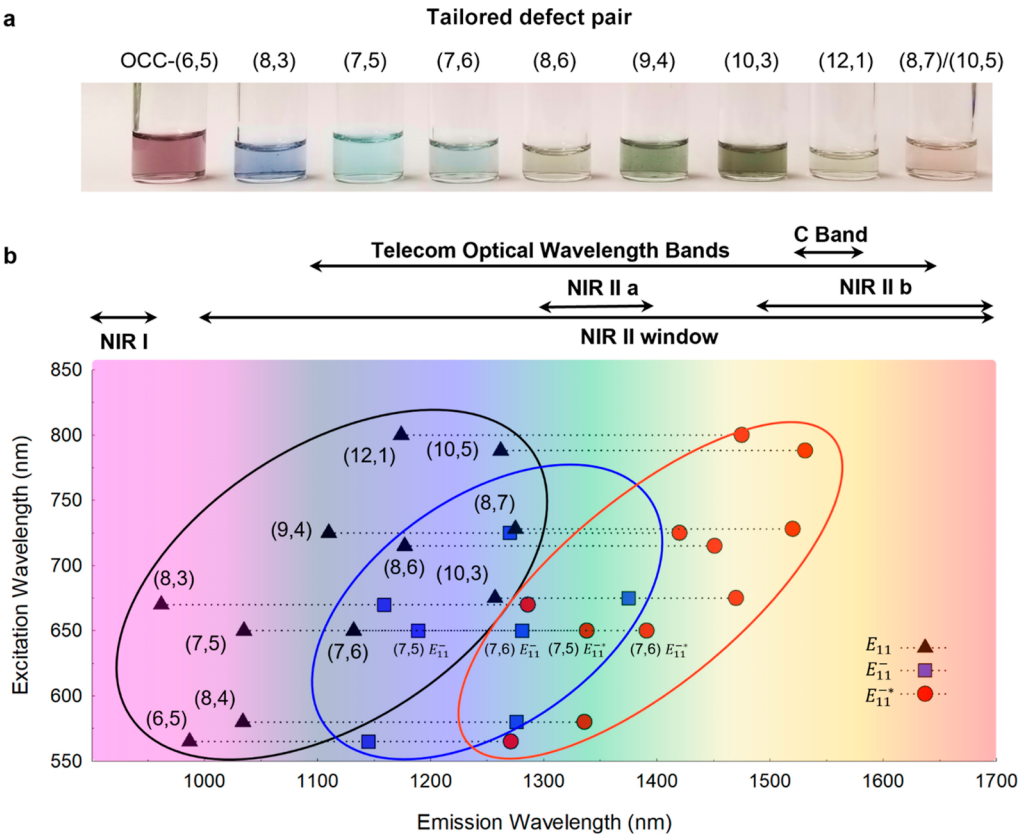

Figure 4. Defect pair-tailored OCCs cover both the telecom and NIR II spectral windows. (a) Photograph of aqueous solutions of 3F-SO_3-Ar/OH OCC-tailored SWCNTs of different chiralities (shown in parentheses). (b) Summary of the attainable emission wavelengths for E_{11} (black triangles), E_{11}^- (blue squares), and E_{11}^-* (red circles). The E_{11}^- and E_{11}^-* data points from (7,5) and (7,6) OCC-SWCNTs are labeled for clarity, as their excitation wavelengths are similar.

weak nucleophilicity or increased steric hindrance[31] that could make the defect pair thermodynamically unstable.

Having determined the critical role of nucleophilic solvents in this diazonium chemistry, we then sought to explore how combinations of different diazonium reactants and pairing groups affect the OCC PL (Figure 2). We investigated two aniline precursors, 2,3,4,5,6-pentafluoro-aniline (5F-Ar) and 3,4,5-trifluoro-2-chlorosulfonyl-aniline (3F−SO_2Cl-Ar), the latter of which was chosen for its bulky size, to functionalize the SWCNTs along with different nucleophilic solvents. We chose to focus on these fluorinated aniline compounds because fluorine inhibits the possible sulfonation reaction, thereby simplifying structural assignment and analysis. We confirmed the covalent attachment of 3F-SO_2Cl-Ar by direct analysis in real time mass spectrometry (see Supporting Information and Figure S10-12 for more details). Note that hydrolysis converts 3F-SO_2Cl-Ar in water to 3,4,5-trifluoro-2-sulfonate-aryl (3F-SO_3-Ar) (Figure S12).

Ensemble-level PL measurements showed that some of these aniline−solvent combinations gave rise to a second defect PL peak (labeled E_{11}^-*) located at ∼1240−1270 nm, which is ∼100 meV more red-shifted from the OCC-generated E_{11}^- emission of the (6,5)-SWCNTs. For example, while the 3F-Ar/OH defect pair features one predominant E_{11}^- PL peak (Figure 2a,d), E_{11}^-* begins to emerge in 5F-Ar/OC_2H_5 (Figure 2b,e). Furthermore, ∼90% of the defect PL occurs at E_{11}^-* for nanotubes functionalized by the 3F-SO_3-Ar/*i*-OC_3H_7 defect pair (Figure 2c,f). We note that both E_{11}^- and E_{11}^-* emissions significantly increase with the rising density of the implanted OCCs, which can be controlled *via* the amount of aniline derivative used in the reaction (Figure S13). Importantly, the corresponding PL emission features remain largely unchanged regardless of the evolution of the overall emission intensity (Figure S13). The E_{11}^-* emission also shows outstanding stability and brightness (Figure S14).

Single-nanotube hyperspectral PL imaging was then used to confirm that these different peaks were not due to inhomogeneous functionalization (Figures 2g−i and S15−S17). Figure 2g shows that 3F-Ar/OH defect pairs on individual (6,5)-SWCNTs emit mainly in the wavelength range of ∼1140−1170 nm, as is typical for E_{11}^-. However, 5F-Ar/OC_2H_5 shows a second defect emission located at ∼1250 nm (E_{11}^-*) (Figure 2h). For 3F-SO_3-Ar/*i*-OC_3H_7, the E_{11}^-* peak becomes predominant (Figure 2i). We note that the E_{11}^-* peak for 3F-SO_3-Ar/*i*-OC_3H_7 is red-shifted more substantially than that from the 5F-Ar defects, which may be due to a greater electron-withdrawing capability of the ortho SO_3 group than that of the F group.[32] Histograms of the E_{11}^- and E_{11}^-* emission wavelengths constructed from single-nanotube PL imaging closely match the ensemble measurement from the corresponding bulk solution samples (Figure 2j−l), unambiguously showing that both E_{11}^- and E_{11}^-* indeed originate from the OCCs synthesized on the SWCNTs.

We further found that the steric hindrance effect of the defect pair was strongly correlated with the ratio of the E_{11}^- and E_{11}^-* emissions. A functional group can rotate 360° when covalently attached to the sp^2 carbon lattice through a single C−C bond. The radius of this rotation defines the steric size of

https://doi.org/10.1021/jacs.2c03846
J. Am. Chem. Soc. 2022, 144, 13234−13241

the functional group. We constructed topographic steric maps[33] of different aryl (3F-Ar, 5F-Ar, 3F-SO_3-Ar) and pairing groups (−OH, $-OCH_3$, $-OC_2H_5$, $-OC_3H_7$, $-i$-OC_3H_7) to compare their steric sizes (Figure 3). It is important to note that due to the $-SO_3^-$ substituent on the aryl ring, 3F-SO_3-Ar is sterically larger than 5F-Ar and 3F-Ar. Although 5F-Ar and 3F-Ar appear identical from the top view, sterically 5F-Ar is still ∼0.4 Å larger than 3F-Ar as the ortho fluorine atom is larger than hydrogen. Note also that the 3F-Ar/$-i$-OC_3H_7 pair did not lead to observable defect PL for unknown reasons. We plotted the integrated area of the E_{11}^- and E_{11}^-* emissions as a function of the steric sizes (Figure 3) and found a positive correlation that larger functional groups lead to a higher percentage of E_{11}^-*. Note that in this simple model we did not consider the curvature of the nanotube host, but the trend as revealed in Figure 3 clearly points to a steric hindrance effect. Notably, ∼90% of the defect emission is E_{11}^-* for the largest defect pair 3F-SO_3-Ar/i-OC_3H_7, representing a stark contrast to 3F-Ar/OH, the smallest pair studied here, which predominately shows E_{11}^- emission. Although the steric impact was previously reported on a different OCC system,[21] the high selectivity we observed here is notable. To find a possible explanation for these observations, we performed DFT calculations (see the Supporting Information for details) and found that para bonding configurations tended to become more stable relative to the ortho configurations as the size of either the aryl or the pairing group increased (Figure S18). This pattern closely follows our experimental observation of increasingly stronger E_{11}^-* emission than E_{11}^- as the size of the OCC defect pair increased. This suggests that we can assign the E_{11}^-* emission to the para bonding configurations, whereas the E_{11}^- peak corresponds to OCCs with an ortho bonding configuration.

The phenomena we observed extend well beyond a specific nanotube chirality and apply to at least the 11 SWCNT species we studied (Figures S19−S21). Figure 4a shows photographs of chirality sorted OCC-SWCNTs that feature the 3F−SO_3-Ar/OH defect pairs. All these OCC-SWCNTs exhibit predominantly E_{11}^-* defect emission that is ∼250−360 meV red-shifted from the E_{11} emission of the pristine nanotubes (Figure S22). Figure S23 summarizes the percentage of E_{11}^-* and E_{11}^- emission from 3F-SO_3-Ar/OH defect pairs added to different nanotube chiralities, which shows that this bulky defect pair causes excitons to predominately channel to the E_{11}^-* states regardless of the nanotube host structure. Figure 4b maps the wavelengths of the E_{11}, E_{11}^-, and E_{11}^-* emission peaks observed in this study. The E_{11}^-* emission spans from ∼1240 to ∼1600 nm, which effectively covers the NIR IIa and IIb windows that can enable high-resolution deep tissue imaging.[34−36] Furthermore, the E_{11}^-* emission also covers the wavelengths used for telecom communications.[9,14] In particular, the 3F-SO_3-Ar/OH defect pairs on (10,5) and (8,7)-SWCNTs show predominate emission peaks at ∼1527 and ∼1536 nm, respectively, which directly fall within the telecom C band (1525−1560 nm) used in fiber communications (Figure S24). We note that although defect emissions beyond 1200 nm have been previously reported by others[9,15] and us,[8] these emission peaks rarely arise as the dominant features as observed here.

CONCLUSIONS

In conclusion, we have found that water plays an unexpected role as a nucleophilic agent that is necessary to complete the aryl diazonium reaction with SWCNTs in chlorosulfonic acid. This finding allowed us to control the pairing groups of OCCs by using a variety of nucleophilic solvents in place of water. We further showed evidence that the atomic configurations of the OCC defect pairs can be spatially controlled based on the steric sizes of the two functional groups, which closely follows the wisdom from organic chemistry but here the functional groups are competing on an extensive lattice. This work provides key insights to understand the chemical nature of the pairing group in the covalent modification of graphitic materials with aryl diazonium chemistry. It also significantly expands the library of OCCs, given the many possible choices of pairing groups, and opens a synthetic pathway to precisely tailor the defect pairs. These findings may broadly impact imaging, sensing, and quantum technologies, where these defect color centers are rapidly emerging as an enabling element.[9,12,13,37,38] In light of our work here, we further propose to re-examine the many covalent chemistries developed for these materials,[2,3,11] particularly the influence of the pairing group under different reaction conditions. It is possible that under different pH conditions (and broadly in terms of the Lewis acid and base concept) both radical and carbocation mechanisms may co-exist, as observed with organic diazonium chemistry, which may impart different pairing groups. We are designing experiments to verify this hypothesis and will report our findings in the future. However, our work here unambiguously shows the incorporation of OH as the pairing group for diazonium reactions involving chlorosulfonic acid and unlocks the possibility to control this pairing group. Furthermore, although our work is focused on SWCNTs and diazonium reactions, one should expect similar questions when breaking a C=C bond in any sp^2 carbon lattices or smaller π conjugated systems during covalent functionalization.

ASSOCIATED CONTENT

Supporting Information

The Supporting Information is available free of charge at https://pubs.acs.org/doi/10.1021/jacs.2c03846.

Methods for SWCNT functionalization, synthesis of 2-amino-4,5,6-trifluorobenezen-1-sulfonyl chloride, chirality sorting of OCC-SWCNTs, spectroscopic characterization and hyperspectral PL imaging of OCC-SWCNTs, experimental setup and spectra for ^{1}H NMR and ^{19}F NMR experiments, experimental setup and spectra of the direct analysis in real time mass spectrometry, DFT calculations, and supplementary tables and notes (PDF)

AUTHOR INFORMATION

Corresponding Author

YuHuang Wang − *Department of Chemistry and Biochemistry, University of Maryland, College Park, Maryland 20742, United States; Maryland NanoCenter, University of Maryland, College Park, Maryland 20742, United State;* orcid.org/0000-0002-5664-1849; Email: yhw@umd.edu

Authors

Peng Wang − *Department of Chemistry and Biochemistry, University of Maryland, College Park, Maryland 20742, United States;* orcid.org/0000-0003-0343-3920

Jacob Fortner − *Department of Chemistry and Biochemistry, University of Maryland, College Park, Maryland 20742, United States*
Hongbin Luo − *Department of Chemistry and Biochemistry, University of Maryland, College Park, Maryland 20742, United States*
Jacek Kłos − *Department of Chemistry and Biochemistry and Department of Physics, Joint Quantum Institute, University of Maryland, College Park, Maryland 20742, United States;* orcid.org/0000-0002-7407-303X
Xiaojian Wu − *Department of Chemistry and Biochemistry, University of Maryland, College Park, Maryland 20742, United States*
Haoran Qu − *Department of Chemistry and Biochemistry, University of Maryland, College Park, Maryland 20742, United States;* orcid.org/0000-0003-4536-6703
Fu Chen − *Department of Chemistry and Biochemistry, University of Maryland, College Park, Maryland 20742, United States*
Yue Li − *Department of Chemistry and Biochemistry, University of Maryland, College Park, Maryland 20742, United States;* orcid.org/0000-0002-1874-2999

Complete contact information is available at: https://pubs.acs.org/10.1021/jacs.2c03846

Author Contributions

[‖]J.F. and H.L. contributed equally to this work.

Notes

The authors declare the following competing financial interest(s): YW, PW, and HL are the inventors of a pending patent application based in part on this work.

■ ACKNOWLEDGMENTS

This work was supported in part by the National Science Foundation (grant no. PHY1839165, CHE1904488, and CHE2204202). We acknowledge the Center for Enhanced Nanofluidic Transport (CENT), an Energy Frontier Research Center funded by the U.S. Department of Energy, and Office of Science, Basic Energy Sciences under Award no. DE-SC0019112 for personnel and instrumentation support. We also gratefully acknowledge the Maryland Advanced Research Computing Center (MARCC) for providing part of the computational resources for the quantum chemical calculations. The authors thank A. Brozena for valuable discussions.

■ REFERENCES

(1) Griefs, P. Vorläufige Notiz über die Einwirkung von salpetriger Säure auf Amidinitro-und Aminitrophenylsäure. *Justus Liebigs Ann. Chem.* **1858**, *106*, 123−125.
(2) Paulus, G. L. C.; Wang, Q. H.; Strano, M. S. Covalent electron transfer chemistry of graphene with diazonium salts. *Acc. Chem. Res.* **2013**, *46*, 160−170.
(3) Bahr, J. L.; Tour, J. M. Covalent chemistry of single-wall carbon nanotubes. *J. Mater. Chem. A* **2002**, *12*, 1952−1958.
(4) Pinson, J.; Podvorica, F. Attachment of organic layers to conductive or semiconductive surfaces by reduction of diazonium salts. *Chem. Soc. Rev.* **2005**, *34*, 429−439.
(5) Ryder, C. R.; Wood, J. D.; Wells, S. A.; Yang, Y.; Jariwala, D.; Marks, T. J.; Schatz, G. C.; Hersam, M. C. Covalent functionalization and passivation of exfoliated black phosphorus via aryl diazonium chemistry. *Nat. Chem.* **2016**, *8*, 597−602.
(6) Niyogi, S.; Bekyarova, E.; Itkis, M. E.; Zhang, H.; Shepperd, K.; Hicks, J.; Sprinkle, M.; Berger, C.; Lau, C. N.; deHeer, W. A.; et al. Spectroscopy of covalently functionalized graphene. *Nano Lett.* **2010**, *10*, 4061−4066.
(7) Assresahegn, B. D.; Brousse, T.; Bélanger, D. Advances on the use of diazonium chemistry for functionalization of materials used in energy storage systems. *Carbon* **2015**, *92*, 362−381.
(8) Piao, Y.; Meany, B.; Powell, L. R.; Valley, N.; Kwon, H.; Schatz, G. C.; Wang, Y. Brightening of carbon nanotube photoluminescence through the incorporation of sp3 defects. *Nat. Chem.* **2013**, *5*, 840−845.
(9) He, X.; Hartmann, N. F.; Ma, X.; Kim, Y.; Ihly, R.; Blackburn, J. L.; Gao, W.; Kono, J.; Yomogida, Y.; Hirano, A.; et al. Tunable room-temperature single-photon emission at telecom wavelengths from sp^3 defects in carbon nanotubes. *Nat. Photonics* **2017**, *11*, 577−582.
(10) Kim, M.; Wu, X.; Ao, G.; He, X.; Kwon, H.; Hartmann, N. F.; Zheng, M.; Doorn, S. K.; Wang, Y. Mapping structure-property relationships of organic color centers. *Chem* **2018**, *4*, 2180−2191.
(11) Brozena, A. H.; Kim, M.; Powell, L. R.; Wang, Y. Controlling the optical properties of carbon nanotubes with organic colour-centre quantum defects. *Nat. Rev. Chem* **2019**, *3*, 375−392.
(12) Mandal, A. K.; Wu, X.; Ferreira, J. S.; Kim, M.; Powell, L. R.; Kwon, H.; Groc, L.; Wang, Y.; Cognet, L. Fluorescent sp^3 defect-tailored carbon nanotubes enable NIR-II single particle imaging in live brain slices at ultra-low excitation doses. *Sci. Rep.* **2020**, *10*, 5286.
(13) Kwon, H.; Kim, M.; Meany, B.; Piao, Y.; Powell, L. R.; Wang, Y. Optical probing of local pH and temperature in complex fluids with covalently functionalized, semiconducting carbon nanotubes. *J. Phys. Chem. C* **2015**, *119*, 3733−3739.
(14) He, X.; Htoon, H.; Doorn, S. K.; Pernice, W. H. P.; Pyatkov, F.; Krupke, R.; Jeantet, A.; Chassagneux, Y.; Voisin, C. Carbon nanotubes as emerging quantum-light sources. *Nat. Mater.* **2018**, *17*, 663−670.
(15) Settele, S.; Berger, F. J.; Lindenthal, S.; Zhao, S.; El Yumin, A. A.; Zorn, N. F.; Asyuda, A.; Zharnikov, M.; Högele, A.; Zaumseil, J. Synthetic control over the binding configuration of luminescent sp^3-defects in single-walled carbon nanotubes. *Nat. Commun.* **2021**, *12*, 2119.
(16) Strano, M. S.; Dyke, C. A.; Usrey, M. L.; Barone, P. W.; Allen, M. J.; Shan, H.; Kittrell, C.; Hauge, R. H.; Tour, J. M.; Smalley, R. E. Electronic structure control of single-walled carbon nanotube functionalization. *Science* **2003**, *301*, 1519−1522.
(17) Schmidt, G.; Gallon, S.; Esnouf, S.; Bourgoin, J.-P.; Chenevier, P. Mechanism of the coupling of diazonium to single-walled carbon nanotubes and its consequences. *Chem.—Eur. J.* **2009**, *15*, 2101−2110.
(18) He, X.; Gifford, B. J.; Hartmann, N. F.; Ihly, R.; Ma, X.; Kilina, S. V.; Luo, Y.; Shayan, K.; Strauf, S.; Blackburn, J. L.; et al. Low-temperature single carbon nanotube spectroscopy of sp^3 quantum defects. *ACS Nano* **2017**, *11*, 10785−10796.
(19) Gifford, B. J.; Kilina, S.; Htoon, H.; Doorn, S. K.; Tretiak, S. Controlling defect-state photophysics in covalently functionalized single-walled carbon nanotubes. *Acc. Chem. Res.* **2020**, *53*, 1791−1801.
(20) Gifford, B. J.; Sifain, A. E.; Htoon, H.; Doorn, S. K.; Kilina, S.; Tretiak, S. Correction scheme for comparison of computed and experimental optical transition energies in functionalized single-walled carbon nanotubes. *J. Phys. Chem. Lett.* **2018**, *9*, 2460−2468.
(21) Shiraki, T.; Shiraishi, T.; Juhász, G.; Nakashima, N. Emergence of new red-shifted carbon nanotube photoluminescence based on proximal doped-site design. *Sci. Rep.* **2016**, *6*, 28393.
(22) Gifford, B. J.; Kilina, S.; Htoon, H.; Doorn, S. K.; Tretiak, S. Exciton Localization and Optical Emission in Aryl-Functionalized Carbon Nanotubes. *J. Phys. Chem. C* **2018**, *122*, 1828−1838.
(23) Kwon, H.; Furmanchuk, A. o.; Kim, M.; Meany, B.; Guo, Y.; Schatz, G. C.; Wang, Y. Molecularly tunable fluorescent quantum defects. *J. Am. Chem. Soc.* **2016**, *138*, 6878−6885.
(24) Aharonovich, I.; Englund, D.; Toth, M. Solid-state single-photon emitters. *Nat. Photonics* **2016**, *10*, 631−641.
(25) Saha, A.; Gifford, B. J.; He, X.; Ao, G.; Zheng, M.; Kataura, H.; Htoon, H.; Kilina, S.; Tretiak, S.; Doorn, S. K. Narrow-band single-

photon emission through selective aryl functionalization of zigzag carbon nanotubes. *Nat. Chem.* **2018**, *10*, 1089−1095.
(26) Qu, H.; Wu, X.; Fortner, J.; Kim, M.; Wang, P.; Wang, Y. Reconfiguring organic color centers on the sp^2 carbon lattice of single-walled carbon nanotubes. *ACS Nano* **2022**, *16*, 2077−2087.
(27) Luo, H.-B.; Wang, P.; Wu, X.; Qu, H.; Ren, X.; Wang, Y. One-pot, large-scale synthesis of organic color center-tailored semiconducting carbon nanotubes. *ACS Nano* **2019**, *13*, 8417−8424.
(28) Hudson, J. L.; Casavant, M. J.; Tour, J. M. Water-soluble, exfoliated, nonroping single-wall carbon nanotubes. *J. Am. Chem. Soc.* **2004**, *126*, 11158−11159.
(29) Cesbron, M.; Dabos-Seignon, S.; Gautier, C.; Breton, T. Enhanced electrocatalytic activity on TEMPO mixed film grafted by diazonium reduction. *Electrochim. Acta* **2020**, *345*, 136190.
(30) Pazo-Llorente, R.; Bravo-Diaz, C.; Gonzalez-Romero, E. pH effects on ethanolysis of some arenediazonium ions: evidence for homolytic dediazoniation proceeding through formation of transient diazo ethers. *Eur. J. Org. Chem.* **2004**, 3221−3226.
(31) Reichardt, C.; Welton, T. *Solvents and Solvent Effects in Organic Chemistry*; John Wiley & Sons, 2011.
(32) Clayden, J.; Greeves, N.; Warren, S. *Organic Chemistry*; Oxford University Press, 2012.
(33) Falivene, L.; Cao, Z.; Petta, A.; Serra, L.; Poater, A.; Oliva, R.; Scarano, V.; Cavallo, L. Towards the online computer-aided design of catalytic pockets. *Nat. Chem.* **2019**, *11*, 872−879.
(34) Hong, G.; Antaris, A. L.; Dai, H. Near-infrared fluorophores for biomedical imaging. *Nat. Biomed. Eng.* **2017**, *1*, 0010.
(35) Hong, G.; Diao, S.; Antaris, A. L.; Dai, H. Carbon nanomaterials for biological imaging and nanomedicinal therapy. *Chem. Rev.* **2015**, *115*, 10816−10906.
(36) Roxbury, D.; Jena, P. V.; Williams, R. M.; Enyedi, B.; Niethammer, P.; Marcet, S.; Verhaegen, M.; Blais-Ouellette, S.; Heller, D. A. Hyperspectral Microscopy of Near-Infrared Fluorescence Enables 17-Chirality Carbon Nanotube Imaging. *Sci. Rep.* **2015**, *5*, 14167.
(37) Kim, M.; Chen, C.; Wang, P.; Mulvey, J. J.; Yang, Y.; Wun, C.; Antman-Passig, M.; Luo, H.-B.; Cho, S.; Long-Roche, K.; et al. Detection of ovarian cancer via the spectral fingerprinting of quantum-defect-modified carbon nanotubes in serum by machine learning. *Nat. Biomed. Eng.* **2022**, *6*, 267−275.
(38) Xu, B.; Wu, X.; Kim, M.; Wang, P.; Wang, Y. Electroluminescence from 4-nitroaryl organic color centers in semiconducting single-wall carbon nanotubes. *J. Appl. Phys.* **2021**, *129*, 044305.

https://doi.org/10.1021/jacs.2c03846
J. Am. Chem. Soc. 2022, 144, 13234−13241